Highly Conductive Porous Graphene/Ceramic Composites for Heat Transfer and Thermal Energy Storage

Mi Zhou, Tianquan Lin, Fuqiang Huang, Yajuan Zhong, Zhou Wang, Yufeng Tang, Hui Bi, Dongyun Wan, and Jianhua Lin**

A novel architecture of 3D graphene growth on porous Al_2O_3 ceramics is proposed for thermal management using ambient pressure chemical vapor deposition. The formation mechanism of graphene is attributed to the carbothermic reduction occurring at the Al_2O_3 surface to initialize the nucleation and growth of graphene. The graphene films are coated on insulating anodic aluminum oxide (AAO) templates and porous Al_2O_3 ceramic substrates. The graphene coated AAO possesses one-dimensional isolated graphene tubes, which can act as the media for directional thermal transport. The graphene/Al_2O_3 composite (G-Al_2O_3) contains an interconnected macroporous graphene framework with an extremely low sheet electrical resistance down to 0.11 Ω sq^{-1} and thermal conductivity with 8.28 W m^{-1} K^{-1}. The G-Al_2O_3 provides enormous conductive pathways for electronic and heat transfer, suitable for application as heat sinks. Such a porous composite is also attractive as a highly thermally conductive reservoir to hold phase change materials (stearic acid) for thermal energy storage. This work displays the great potential of CVD direct growth of graphene on dielectric porous substrates for thermal conduction and electronic applications.

1. Introduction

Graphene has received significant attention due to unique electrical, optical and thermal transport properties.[1–6] The electrical and optical properties and related applications have intensively been investigated. The extremely high thermal conductivity (5150 W m^{-1} K^{-1})[4] and electrical conductivity may make graphene be used as fillers in porous ceramic matrix to provide enhanced thermal properties and replace metal or graphite parts in thermal management systems, e.g., heat sinks of light-emitting diode (LED) and electronic devices. Due to the fact that thermal conduction mainly relies on the highly electrically conductive surfaces of graphite, the single-layer graphene with high specific surface area (>2600 m^2 g^{-1})[7] is superior to graphite as a thermal conductor.[8] Porous ceramics can provide ample surfaces for graphene growth to form porous graphene/ceramic composites with excellent thermal transport properties. However, such a porous composite has not been reported, not to mention its applications in thermal management.

The chemically-bonded interface of the graphene/ceramic composites is important for such applications, and chemical vapor deposition (CVD) is a desired method for graphene growth. Recently, the CVD graphene films were able to be grown on various substrates, including metals (e.g., Cu, Ni),[9,10] semiconductors (e.g., Si, SiC),[11] and insulators (e.g., BN, SiO_2).[12,13] Conventional LED heat sinks are made from Al metal, Al_2O_3, and AlN, and ceramic sinks are more and more frequently used by industry due to light weight and high thermal conductivity. Good thermal management of the graphene/ceramic configuration can be expected due to high carrier thermal conductivity from highly electrically conductive graphene and high lattice thermal conductivity from the ceramic substrate.

Three dimensional (3D) graphene was prepared on a porous Ni substrate by using CVD method, and the low electrical resistance and high electrical conductivity of graphene achieved at 0.45 Ω sq^{-1} and 10 S cm^{-1} due to the continuous and chemically-bonded network.[14,15] However, no attempts have been reported to grow 3D graphene on a porous ceramic (Al_2O_3, etc.) to enhance electrical and thermal conductivity. There have also been few investigations on growing graphene on two dimensional (2D) Al_2O_3 substrates.[16] However, such a porous composite of graphene/Al_2O_3 is attractive not only for heat sinks (direct thermal transport, etc.) but also for highly thermally conductive reservoir to hold phase change materials (stearic acid, low-melt-point alloy, etc.) for thermal energy storage.

In this study, a novel architecture of 3D graphene growth on porous Al_2O_3 ceramics is proposed. The graphene films were first grown directly on anodic aluminum oxide templates

M. Zhou, T. Lin, Prof. F. Huang, Dr. Y. Zhong, Z. Wang, Dr. Y. Tang, Dr. H. Bi, Dr. D. Wan
CAS Key Laboratory of Materials for Energy Conversion
Shanghai Institute of Ceramics
Chinese Academy of Sciences
Shanghai 200050, P. R. China
E-mail: huangfq@mail.sic.ac.cn

M. Zhou, T. Lin, Prof. F. Huang, Prof. J. Lin
Beijing National Laboratory for Molecular Sciences and State Key Laboratory of Rare Earth Materials Chemistry and Applications
College of Chemistry and Molecular Engineering
Peking University
Beijing 100871, P. R. China
E-mail: jhlin@pku.edu.cn

DOI: 10.1002/adfm.201202638

(AAO) and porous Al_2O_3 ceramics by using a versatile ambient pressure CVD method (see the Experimental Section). The graphene coated AAO sample (G-AAO) consists of one-dimensional isolated graphene tubes, which can be acted as the media for directional thermal transport. The porous graphene/Al_2O_3 composite (G-Al_2O_3) shows an interconnected macroporous framework of graphene sheets, which provides enormous conductive pathways for electronic conduction and thermal transfer. For example, the G-Al_2O_3 sample possesses an extremely low sheet electrical resistance down to 0.11 Ω sq^{-1} and the thermal conductivity of 8.28 W m^{-1} K^{-1}. Furthermore, a phase change material of 3D graphene/Al_2O_3/stearic acid composite (SA-G-PAO) is assembled for the purpose of thermal energy storage.

2. Results and Discussion

2.1. Graphene Tubes/AAO Composite

The AAO template is a regular one-dimensional channel array with average pore size (d) of ≈100 nm and pore center to center distance (d') of ≈125 nm, as shown in Supporting Information Figure S1a. Such AAO templates were shrunk to be one with d = 95 nm and d' = 115 nm after firing at 1200 °C for 2 h to ensure no further shrinkage during the graphene growth. The graphene was grown at 1200 °C for 30 min under the flow of Ar, H_2, and CH_4 (Ar:H_2:CH_4 = 450:50:10 sccm), and the regular pore array is shown in **Figure 1**a,b. The graphene sheets grew around the surface of AAO channel and some sheets were extended out into the channel as shown Figure 1c,d. The high-resolution transmission electron microscopy (HRTEM) image of the folded graphene edge clearly reveals the bilayer feature of the graphene sheets.

To further characterize the structure, the AAO template was etched using HF/H_3PO_4 mixed solution (mole ratio 1:1) to obtain the graphene tubes. As shown in Figure 1e, the isolated graphene tubes were clearly observed by TEM. From the TEM images, the diameter of the isolated graphene tubes is estimated to be 80–120 nm, which is closed to the pore size of AAO template (≈100 nm).

Raman spectroscopy is a powerful nondestructive tool to determine quality and layer number of graphene. The typical Raman spectrum of the G-AAO reveals the G peak at ≈1590 cm^{-1} and the 2D peak at ≈2690 cm^{-1} with a comparable intensity, as shown in Figure 1f. The full-width at half-height maximum (FWHM) of the 2D peak is about 55 cm^{-1}. Raman spectra taken from tens of spots in different regions show similar features with the 2D band FWHM of 40–60 cm^{-1} and I_G/I_{2D} of 0.8–1.6. Furthermore, the 2D peak (inset of Figure 1f) is asymmetric and can be deconvoluted into four small peaks: $2D_{1B}$, $2D_{1A}$, $2D_{2A}$, and $2D_{2B}$, individually with FWHM of 30 to 35 cm^{-1}, which correspond to four permissible photon transitions in graphene.[17,18] All these data indicate that the graphene grown on AAO is indeed bilayered, which is consistent with the previous reports of bilayer graphene.[19–24] The D peak at ≈1340 cm^{-1} is derived from defects or edges of graphene, similar to the reported results.[24] From the above investigation, it reveals that bilayer graphene is able to directly grow fully around the surface of AAO channel.

The one-dimensional (1D) isolated graphene tubes grown on AAO channels is conductive along the tubes to be acted as the media for directional electronic and thermal transport. The electronic conductivity of G-AAO along the tube direction is ≈950 S m^{-1}, much higher than that of the direction vertical to the channel (4.3 S m^{-1}). Therefore, the advantage along those tubes of the G-AAO may open up a new avenue for directional electronic and thermal transport of heat sink in limited small space.

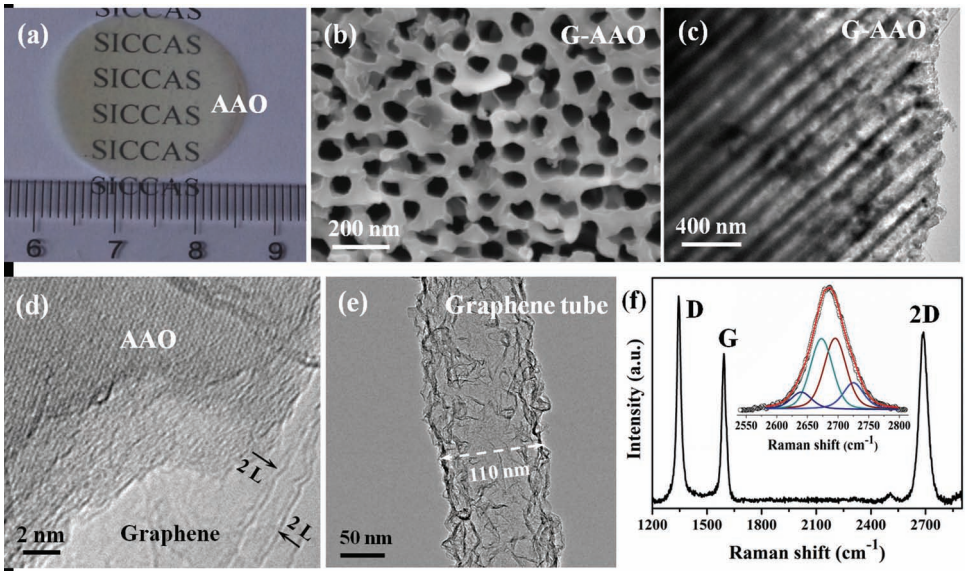

Figure 1. a) Photograph of anodic aluminum oxide (AAO). b) SEM, c) TEM and d) HRTEM images of graphene-coated anodic aluminum oxide (G-AAO) grown at 1200 °C for 30 min. e) TEM image and f) Raman spectrum of graphene tubes after etching of AAO template. The inset shows that the 2D peak can be deconvoluted into four components: $2D_{1B}$, $2D_{1A}$, $2D_{2A}$, and $2D_{2B}$ from the left to the right.

2.2. Three-dimensional Graphene/Al_2O_3 Composite

The array in the G-AAO composite consists of isolated graphene tubes without a 3D interconnected graphene network, which can only act as media for directional thermal transport and not as an excellent 3D heat sink. However, the AAO-assisted preparation still draws a clear direction towards the 3D continuous graphene growth on a porous Al_2O_3 substrate. With the aid of ceramic process, the porous Al_2O_3 ceramics were sintered at 1300 °C for 3 h. The porous Al_2O_3 ceramic is composed of anomalous Al_2O_3 grains connected with each other to form a 3D interconnected network (**Figure 2**a,b). Three graphene/Al_2O_3 (G-Al_2O_3) samples were prepared at 1200 °C for 30, 60, and 120 min, as shown in Supporting Information Figure S3.

The thickness of the obtained graphene was demonstrated by the HRTEM image displayed in Figure 2c, which reveals that the bilayer graphene sheets are tightly coated on the surface of Al_2O_3. The graphene sheets were removed from the Al_2O_3 substrate using HF/H_3PO_3 etching, and then transferred onto TEM grids for further characterization. The bilayer structure confirmed by HRTEM (Figure 2d) of the folded edges of graphene sheets agrees well with the Raman spectroscopic data. The SAED pattern in Figure 2e displays the typical hexagonal crystalline structure of graphene. A 6° rotation found between the two layers suggests non-AA or AB-stacked bilayer graphene.

The thickness and quality of graphene was also examined by the Raman spectroscopy. In the 30-min-grown sample, the intensity ratio of 2D and G bands ($I_{2D}/I_G \approx 1.2$) and the FWHM of the 2D band (≈60 cm^{-1}) indicate mainly from the two-layer graphene, as shown in Figure 2f. With increasing growth time, the defects of graphene are significantly reduced, as illustrated in Figure 2f, and the layer number of graphene increases. According to the I_{2D}/I_G ratio of Raman spectra and the HRTEM images of the folded edges (Supporting Information Figure S3), the layer number of the 60-min-grown graphene are few-layered (<10 layers), and the 120-min-grown graphene becomes ultrathin graphite (≈15–20 layers). The anomalous Al_2O_3 grains are stack with each other to form plenty of interconnected pores (see Figure 2b). The porous structure makes the G-Al_2O_3 possess a larger surface area and more transport channels, which are beneficial for forming a continuous interconnected graphene network for electronic and thermal transport. The pore size and distribution of Al_2O_3 are adjustable by changing ceramic processing, and the graphene quality is controllable by tuning the CVD growth time and the gas flow rate. Therefore, the optimal microstructure of the 3D graphene/Al_2O_3 composite promises excellent electrical transport and thermal conductive properties.

2.3. Growth Mechanism of Graphene on Al_2O_3 Substrate

In order to explore the formation mechanism of graphene directly grown on Al_2O_3, HRTEM, and X-ray photoelectron spectroscopy (XPS) analyses were performed. The two-layered graphene directly rooting on the Al_2O_3 lattice fringes have an interspacing of ca. 0.34 nm, as shown in Figure 2c. Although the lattice mismatch between graphene and the Al_2O_3 (012) plane (0.348 nm) is not large, there is no evidence to suggest that the graphene layers align themselves with the Al_2O_3 (012) plane at the initial growth stage. In order to clarify the nucleation of graphene growth, XPS was performed to determine the composition and bonding type of the 3D G-Al_2O_3 composite. The prominent XPS Al 2p peak at 74.3 eV is assigned to aluminum

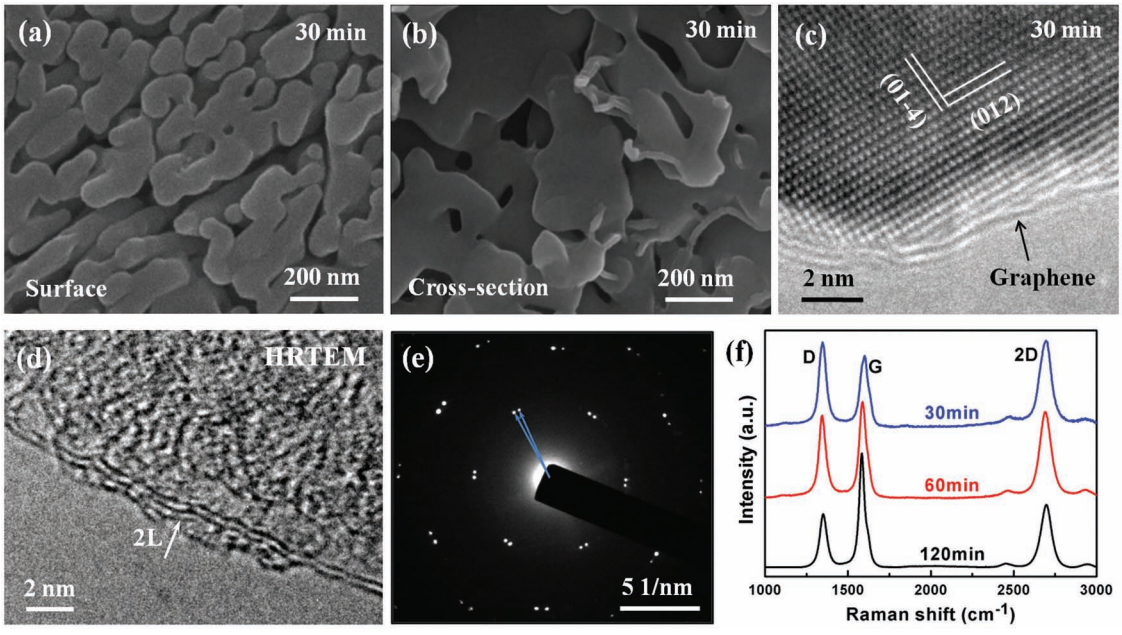

Figure 2. SEM images of a) surface and b) cross-section of graphene-coated Al_2O_3 prepared at 1200 °C for 30 min (30-min-G-Al_2O_3). c) HRTEM image of 30-min-G-Al_2O_3. d) HRTEM image of graphene edge that shows two graphene layers. e) Hexagonal SAED pattern of the bilayer graphene that shows a rotation angle of ≈6° between the two layers. f) Raman spectra of three graphene/Al_2O_3 composites (G-Al_2O_3) growth for 30, 60, and 120 min.

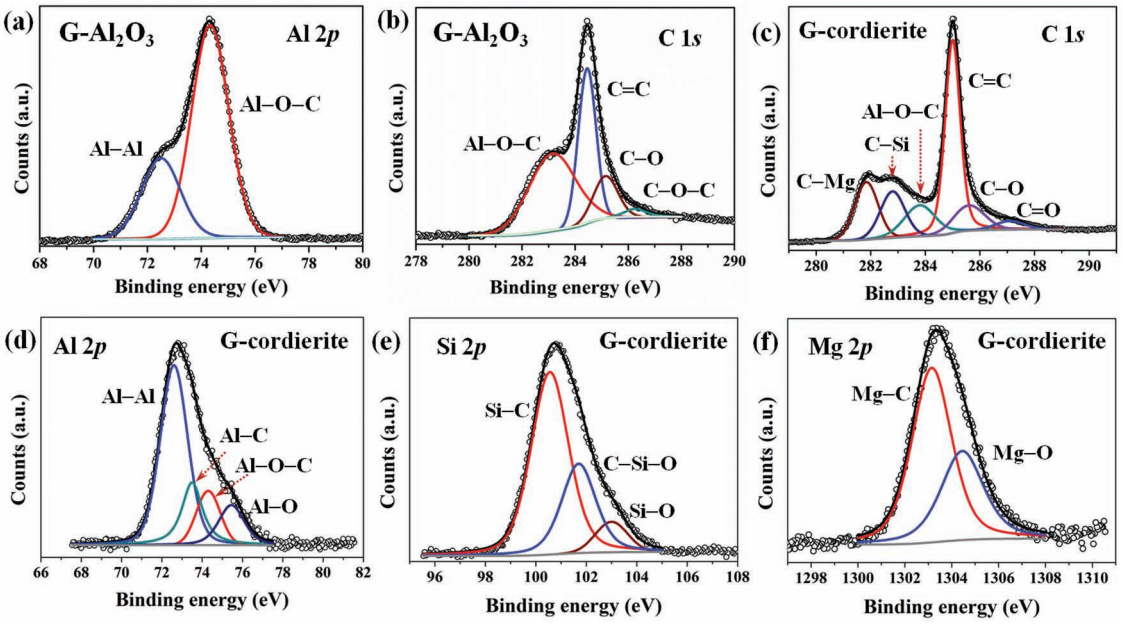

Figure 3. High resolution XPS scans for a) Al 2p and b) C 1s peaks of graphene-coated Al_2O_3 prepared at 1200 °C for 30 min. XPS scans for c) C 1s peaks, d) Al 2p, e) Si 2p, and f) Mg 2p of graphene-coated cordierite prepared at 1200 °C for 30 min.

oxycarbide (Al–O–C) complex[25,26] (**Figure 3**a), and unequivocally indicates the covalent bond formation between graphene and Al_2O_3. The Al 2p shoulder peak at 72.6 eV is contributed to Al–Al bonds.[27,28] The C 1s peak shown in Figure 3b can also be fitted with the binding energies of 283.2 and 284.5 eV, which correspond to the Al–O–C and C=C bonds, respectively.[25,26] The C 1s signal is broadened with small tails at the higher binding energy region corresponding to edge hydroxide (285.2 eV) and ether groups (286.3 eV).

The XPS spectra reveal the existence of Al–O–C, Al–C, Al–Al, and C=C bonds on the surface of Al_2O_3. Apparently, the traditional carbothermic reduction occurred at the Al_2O_3 surface and played an important role in the initial growth of graphene. Therefore, the growth mechanism may be that the activated carbon and hydrogen atoms from the methane decomposition partially reduce the Al_2O_3 surface to form Al–O–C, Al–C and Al–Al bonds. These bonded C atoms as the nucleation centers lead to the segregation of the graphene-like structures.[16] The graphene-like structure is capable to capture nascent carbon atoms and grow up. Therefore, the graphene sheets may be independent on the planes of Al_2O_3, different from the manner in which graphitic layers formed anchor to *h*-BN,[29] ZnS ribbons[30] and MgO.[31] The proposed growth mechanism initialed by carbothermic reduction favors graphene sheets tightly binding to the surfaces of Al_2O_3 grains to achieve better thermal conduction properties (**Figure 4**).

In order to further prove the mechanism, other porous aluminate ceramics, e.g., cordierite ($Mg_2Al_3[AlSi_5]O_{18}$), were used to grow graphene by using the same growth conditions. The graphene were coated on the cordierite substrate displayed in Supporting Information Figure S4. The G peak position at 1585 cm^{-1}, intensity ratio of 2D and G bands ($I_{2D}/I_G \approx 1.05$) in Raman spectrum and the FWHM of the 2D band (≈70 cm^{-1}) indicate that two- or three-layer graphene was obtained, as shown in Supporting Information Figure S4d. This is further demonstrated by the HRTEM image for the folded edges of the three-layered graphene shown in Supporting Information Figure S3c. By the above investigation, it is demonstrated that graphene is also able to directly grow on the cordierite surface. We also investigated the formation mechanism of graphene directly grown on cordierite (G-cordierite) using XPS analysis. The Al–C bonds, aluminum oxycarbide (Al–O–C) complex in Al 2p peak, Al–O–C complex in C 1s peak, Si–C in Si 2p peak and Mg–C bonds in Mg 2p peak presented in G-cordierite. This result confirms that traditional carbothermic reduction occurred on the surface of cordirite and played an important role in the initial growth of graphene.

2.4. Charge and Thermal Transport

The electrical and thermal characteristics of the G-Al_2O_3 are the key for the further thermal management applications. The electrical conductivities of the graphene/Al_2O_3 (G-Al_2O_3) composites were measured by a standardized "four-point probe" setup in order to eliminate contact resistance, and each sample was measured three times to obtain an average value, as listed in **Table 1**. The sheet resistance (R_s) of the vertical to the graphene tubes of 30-min-G-AAO composite is 1649 Ω sq^{-1}, but that of the 30-min-G-Al_2O_3 composite abruptly decreases to 4.35 Ω sq^{-1}, although the conditions of graphene growth are the same. As discussed above, the microstructure of graphene in G-AAO is not a 3D interconnected network except for the nearly isolated graphene tubes, and thus, a high resistance can be expected. The G-Al_2O_3 possesses a 3D interconnected network of electron transport pathways, as confirmed by scanning electron

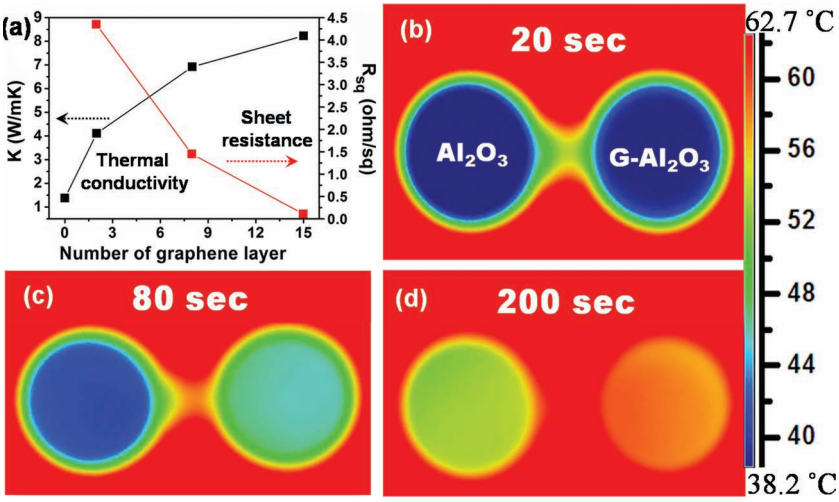

Figure 4. a) Thermal conductivity and sheet resistance of the G-Al_2O_3 as a function of graphene layer number. b–d) Thermal transport evolution of the Al_2O_3 and G-Al_2O_3 ceramic samples.

microscopy (SEM) (Figure 2). Compared with the 2D graphene on the surface of fully dense substrate, the rich macroporosity and multidimensional electron transport pathways of graphene in this 3D interconnected systems ensure the low resistance of the samples. The sheet resistance of 120-min-G-Al_2O_3 is further reduced to 0.11 Ω sq^{-1} due to less defective graphene, which is much lower compared with the 3D graphene assembled from CVD graphene or reduced graphene oxide.[15]

The excellent electrical conductivity of the G-Al_2O_3 composite is contributed to its rich macroporosity and multidimensional electron transport pathways. Such a unique structure brings out excellent thermal transfer properties. As shown in Figure 4a, the effective thermal conductivity of the G-Al_2O_3 increases with the growth time. All kinds of Al_2O_3 were converted to α-Al_2O_3 during the heat treatment process at 1300 °C for 3 h, confirmed by X-ray diffraction (XRD) shown in Supporting Information Figure S5. The thermal conductivity of G-Al_2O_3 was enhanced significantly from 1.84 (0 min) to 8.28 W m^{-1} K^{-1} (120 min), as listed in Table 1. The increased thermal transport property of G-Al_2O_3 is clearly illustrated by thermal images. Temperature distribution images of the Al_2O_3 and G-Al_2O_3 at 20, 80, and 200 s are shown in Figure 4b–d, respectively. The color of G-Al_2O_3 changed quickly from blue to red, faster than that of Al_2O_3, which illustrates the 3D interconnected graphene improves the thermal transport of Al_2O_3 ceramic. The same phenomenon has also been verified in the cooling process (Supporting Information Figure S6). The above results provide strong evidence that 3D graphene leads to an enhancement of the thermal conductivity of G-Al_2O_3. The good interconnected network of the graphene at the interfaces and throughout the G-Al_2O_3 offers a "short cut" for heat transferring, similar to that of carbon foam.[32–34] High thermal conductivity of graphene allows rapid heat transfer throughout the G-Al_2O_3. These results all support the earlier claim of fewer defects in our films.

Table 1. Thermophysical properties (thermal diffusivity α; thermal conductivity κ) and electrical properties (sheet resistance R_s; electrical conductivity σ) of the samples.

Sample	Graphene	R_s [Ω sq^{-1}]	σ [S m^{-1}]	α [mm^2 s^{-1}]	κ [W m^{-1} K^{-1}]
AAO[a)]	–	$>10^7$	$<10^{-7}$	–	–
G-AAO VT[b)]	2 layer	1649	4.3	–	–
G-AAO AT[c)]	2 layer	–	950	–	–
Al_2O_3	–	$>10^7$	$<10^{-7}$	1.07	1.84
30-min-G-Al_2O_3	2 layer	4.35	32.8	2.61	4.49
60-min-G-Al_2O_3	8 layer	1.45	98.5	4.27	7.35
120-min-G-Al_2O_3	>10 layer	0.11	1290	4.81	8.28

[a)]AAO was heated at 1200 °C for 2 h.; [b)]VT: vertical to the graphene tube direction.; [c)]AT: along the graphene tube direction.

2.5. Thermal Energy Storage

Such a porous graphene/ceramic composite is attractive not only for heat sinks but also for highly thermally conductive reservoirs to hold phase change materials for thermal energy storage. As a phase change material, for example, stearic acid (SA) is infiltrated into the porous alumina in an attempt to enhance the thermal conductivity of the thermal energy storage system. The G-AAO samples do not contain interpenetrated conductive pathways, and the G-Al_2O_3 samples do not possess enough large pores to accommodate a large amount of phase change material. Large macroporous ceramic (alumina or cordierite) with a pore size of ≈500 μm was selected to prepare a 3D graphene-coated ceramic composite and further infiltrated with SA to form a SA/graphene/ceramic composite, as shown in **Figure 5**a,b.

The graphene growth again relies on the carbothermic reduction of Al_2O_3 at the same CVD condition (60 min at 1200 °C). The sheet resistance (R_s) of graphene-coated large porous ceramic (G-PAO) is below 20 Ω sq^{-1}, which can be adjusted by changing the microstructure of porous ceramic. Temperature distribution images during the heating time of 30, 60, and 120 s are shown in Figure 5d–f for the composites of ceramic/SA and ceramic/graphene/SA. Temperature distribution is almost the same during the first 20 s (Supporting Information Figure S7). Upon increasing the heating time, the graphene-coated composite had a faster thermal response than the uncoated composite. High thermal conductivity of the 3D graphene coating in the composites allows heat to transfer rapidly throughout the SA. The differential scanning calorimetry (DSC) thermograms for the graphene-coated composite phase change materials before and after the thermal cycling are given in Figure 5c. Heat is stored by SA in the composite during periods of high power operation, and heat is released from the system during periods of

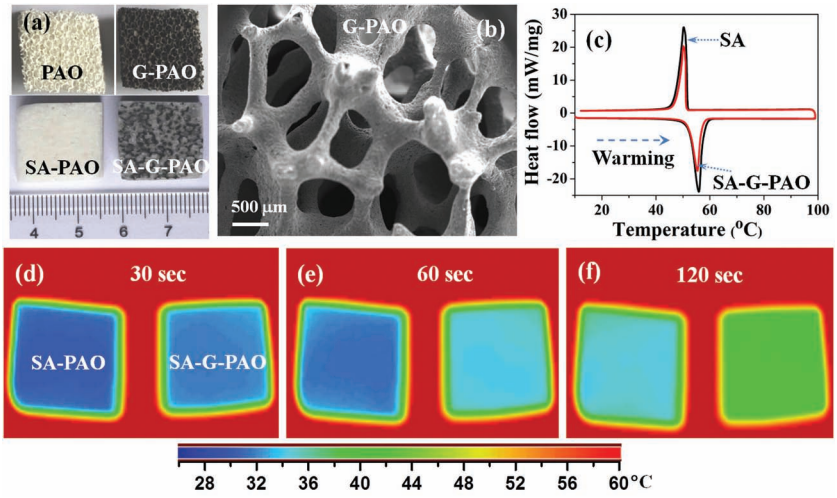

Figure 5. a) Photographs of large porous alumina (PAO), graphene-coated porous alumina (G-PAO), stearic acid (SA)-filled porous alumina (SA-PAO), and SA-G-PAO. b) SEM image of G-PAO. c) DSC curves of SA and SA-G-PAO composite. d–f) Thermal transport evolution of SA-PAO and SA-G-PAO. The thermal images visually illustrate the excellent thermal characteristics of the G-PAO.

reduced power operation by the latent heat effect. The SA and the SA/graphene/ceramic composite have a latent heat of 186 and 130 J/g, respectively. The later depended on the amount of the SA filled in the matrices. The as-prepared porous graphene/ceramic composites have potential applications as a thermal management material in the electronic device.

3. Conclusion

A versatile catalyst-free approach is proposed to directly grow large-area 3D graphene on AAO, micro-pore Al_2O_3 ceramic, and large-pore Al_2O_3 ceramic (PAO) by atmospheric pressure CVD method. The formation mechanism of graphene is based on the carbothermic reduction occurring at the Al_2O_3 surface to initiate the nucleation and growth of graphene. The graphene coated AAO (G-AAO) containing one-dimensional isolated graphene tubes is conductive along the tubes, which can act as a medium for directional thermal transport. The porous graphene/Al_2O_3 composite (G-Al_2O_3) shows an interconnected macroporous framework of graphene sheets with an extremely low sheet electrical resistance down to 0.11 Ω sq^{-1} and thermal conductivity with 8.28 W m^{-1} K^{-1}. The G-Al_2O_3 provides enormous conductive pathways for electronic and thermal transport, suitable for heat sinks. Such a porous composite of G-Al_2O_3 is also attractive as a highly thermally conductive reservoir to hold phase change materials (stearic acid) for thermal energy storage, and the phase change material was assembled by stearic-acid-filled PAO. These graphene-coated porous Al_2O_3 composites may play important role in thermal management applications.

4. Experimental Section

3D Graphene Preparation: The AAO samples were heated at 1200 °C for 2 h to ensure no further shrinkage during the graphene growth. Porous Al_2O_3 ceramic samples were prepared by traditional ceramic technique from Al_2O_3 powders (99.99%, SinoReag). The ceramic green bodies were pressed from the φ 2.5 cm die at 8 MPa, and the final ceramic samples were sintered at 1300 °C for 3 h. The large porous Al_2O_3 ceramic pieces were finally sintered at 1300 °C for 3 h in air by using the polymeric sponge method, as describe elsewhere.[35] Other porous aluminate ceramics such as cordierite ($Mg_2Al_3(AlSi_5)O_{18}$) can also be used to grow graphene by using the same growth conditions.

The samples were placed in the center of a horizontal Al_2O_3 tube mounted inside a high-temperature furnace at 1200 °C with Ar:H_2:CH_4 = 450:50:10 sccm for different times. After the graphene growth, the CH_4 gas flow was shut down, and the samples were cooled down to 500 °C at a rate of 10 °C min^{-1} at the same flow rates of H_2 and Ar as the growth stage. The G-AAO and G-Al_2O_3 with two-layer graphene were prepared under the same conditions with Ar:H_2:CH_4 = 450:50:10 sccm at 1200 °C for 30 min, and the two other G-Al_2O_3 samples were prepared at the same gas flow rate for 60 and 120 min. The large porous G-Al_2O_3 was prepared at 1200 °C for 60 min.

The isolated graphene tubes were removed from the AAO substrate using HF/H_3PO_3 mixed solution (molar ratio 1:1) etching for two days, and then transferred onto TEM grids for further characterization. The AAO template cannot not be removed from the graphene-coated AAO after two weeks by acid etching if the graphene coating is not partially damaged.

Characterization and Measurement: The sample morphology was investigated using a Hitachi S-4800 field emission scanning electron microscope. High resolution transmission electron microscopy images and selected area electron diffraction patterns of graphene were performed on a JEOL 2100F microscope. Raman spectra were collected on a thermal dispersive spectrometer using a laser with an excitation wavelength of 532 nm at a laser power of 10 mW. The electrical transport properties were measured by the Van der Pauw method with an Accent HL5500. Temperature distribution images of the samples were recorded by a thermal imager (sc305, Flir Systems USA). DSC thermogram was tested on the Q100 Thermal Analysis. The thermal transfer properties of G-Al_2O_3 were measured at room temperature by a LFA427 laser conductometer. XPS experiments were carried out on a RBD upgraded PHI-5000C ESCA system (Perkin Elmer) with Mg Kα radiation ($h\nu$ = 1253.6 eV).

Supporting Information

Supporting Information is available from the Wiley Online Library or from the author.

Acknowledgements

M.Z. and T.Q.L. contributed equally to this work. Financial support from National 973 Program of China (Grant no. 2009CB939900), Graphene Project of CAS (Grant no. KGZD-EW-303), NSF of China (Grant nos. 51202275, 11274328, 51121064, 61106088, 21101164, 61076062, 51102263), and STC of Shanghai (Grant no. 10JC1415800).

Received: September 12, 2012
Published online: December 2, 2012

[1] K. S. Novoselov, A. K. Geim, S. V. Morozov, D. Jiang, Y. Zhang, S. V. Dubonos, I. V. Grigorieva, A. A. Firsov, *Science* **2004**, *306*, 666.
[2] A. K. Geim, K. S. Novoselov, *Nat. Mater.* **2007**, *6*, 183.

[3] R. R. Nair, P. Blake, A. N. Grigorenko, K. S. Novoselov, T. J. Booth, T. Stauber, N. M. R. Peres, A. K. Geim, *Science* **2008**, *320*, 1308.
[4] A. A. Balandin, S. Ghosh, W. Bao, I. Calizo, D. Teweldebrhan, F. Miao, C. N. Lau, *Nano Lett.* **2008**, *8*, 902.
[5] A. A. Balandin, *Nat. Mater.* **2011**, *10*, 569.
[6] Z. Yan, G. Liu, J. M. Khan, A. A. Balandin, *Nat. Commun.* **2012**, *3*, 827.
[7] M. D. Stoller, S. Park, Y. Zhu, J. An, R. S. Ruoff, *Nano Lett.* **2008**, *8*, 3498.
[8] M. T. Pettes, H. Ji, R. S. Ruoff, L. Shi, *Nano Lett.* **2012**, *12*, 2959.
[9] X. Li, W. Cai, J. An, S. Kim, J. Nah, D. Yang, R. Piner, A. Velamakanni, I. Jung, E. Tutuc, S. K. Banerjee, L. Colombo, R. S. Ruoff, *Science* **2009**, *324*, 1312.
[10] K. S. Kim, Y. Zhao, H. Jang, S. Y. Lee, J. M. Kim, K. S. Kim, J.-H. Ahn, P. Kim, J. Y. Choi, B. H. Hong, *Nature* **2009**, *457*, 706.
[11] C. Berger, Z. Song, X. Li, X. Wu, N. Brown, C. Naud, D. Mayou, T. Li, J. Hass, A. N. Marchenkov, E. H. Conrad, P. N. First, W. A. de Heer, *Science* **2006**, *312*, 1191.
[12] X. Ding, G. Ding, X. Xie, F. Huang, M. Jiang, *Carbon* **2011**, *49*, 2522.
[13] T. Lin, Y. Wang, H. Bi, D. Wan, F. Huang, X. Xie, M. Jiang, *J. Mater. Chem.* **2012**, *22*, 2859.
[14] H. Bi, F. Huang, J. Liang, Y. Tang, X. Lü, X. Xie, M. Jiang, *J. Mater. Chem.* **2011**, *21*, 17366.
[15] Z. Chen, W. Ren, L. Gao, B. Liu, S. Pei, H. M. Cheng, *Nat. Mater.* **2011**, *10*, 424.
[16] S. K. Jerng, D. S. Yu, Y. S. Kim, J. Ryou, S. Hong, C. Kim, S. Yoon, D. K. Efetov, P. Kim, S. H. Chun, *J. Phys. Chem. C* **2011**, *115*, 4491.
[17] L. M. Malard, M. Pimenta, G. Dresselhaus, M. S. Dresselhaus, *Phys. Rep.* **2009**, *473*, 51.
[18] L. M. Malard, J. Nilsson, D. C. Elias, J. C. Brant, F. Plentz, E. S. Alves, A. H. Castro Neto, M. A. Pimenta, *Phys. Rev. B* **2007**, *76*, 201401.
[19] Z. Yan, Z. Peng, Z. Sun, J. Yao, Y. Zhu, Z. Liu, P. M. Ajayan, J. M. Tour, *ACS Nano* **2011**, *5*, 8187.
[20] L. Liu, H. Zhou, R. Cheng, W. Yu, Y. Liu, Y. Chen, J. Shaw, X. Zhong, Y. Huang, X. Duan, *ACS Nano* **2012**, *6*, 8241.
[21] Z. Peng, Z. Yan, Z. Sun, J. M. Tour, *ACS Nano* **2011**, *5*, 8241.
[22] H. Bi, F. Huang, W. Zhao, X. Lü, J. Chen, T. Lin, D. Wan, X. Xie, M. Jiang, *Carbon* **2012**, *50*, 2703.
[23] S. Lee, K. Lee, Z. Zhong, *Nano Lett.* **2010**, *10*, 4702.
[24] A. C. Ferrari, J. C. Meyer, V. Scardaci, C. Casiraghi, M. Lazzeri, F. Mauri, S. Piscanec, D. Jiang, K. S. Novoselov, S. Roth, A. K. Geim, *Phys. Rev. Lett.* **2006**, *97*, 187401.
[25] S. Akhter, X. L. Zhou, J. M. White, *Appl. Surf. Sci.* **1989**, *37*, 201.
[26] B. M. DeKoven, P. L. Hagans, *Appl. Surf. Sci.* **1986**, *27*, 199.
[27] K. Domen, T. J. Chuang, *J. Chem. Phys.* **1989**, *90*, 3318.
[28] I. Olefjord, H. J. Mathieu, P. Marcus, *Surf. Interface Anal.* **1990**, *15*, 681.
[29] C. Bjelkevig, Z. Mi, J. Xiao, P. Dowben, L. Wang, W. N. Mei, J. A. Kelber, *J. Phys.: Condens. Matter* **2010**, *22*, 302002.
[30] D. Wei, Y. Liu, H. Zhang, L. Huang, B. Wu, J. Chen, G. Yu, *J. Am. Chem. Soc.* **2009**, *131*, 11147.
[31] M. H. Rümmeli, A. Bachmatiuk, A. Scott, F. Börrnert, J. H. Warner, V. Hoffman, J. H. Lin, G. Cuniberti, B. Büchner, *ACS Nano* **2010**, *4*, 4206.
[32] J. Klett, R. Hardy, E. Romine, C. Walls, T. Burchell, *Carbon* **2000**, *38*, 953.
[33] N. C. Gallego, J. W. Klett, *Carbon* **2003**, *41*, 1461.
[34] S. Li, Y. Song, J. Shi, L. Liu, X. Wei, Q. Guo, *Carbon* **2007**, *45*, 2092.
[35] M. D. M. Innocentini, P. Sepulveda, V. R. Salvini, V. C. Pandolfelli, J. R. Coury, *J. Am. Ceram. Soc.* **1998**, *81*, 3349.